The International Archives of the Photogrammetry, Remote Sensing and Spatial Information Sciences, Volume L-4/W1-2026
Free and Open Source Software for Geospatial (FOSS4G) 2026 – Academic Track "Bridging Geospatial Technology and Humanity",
30 August–5 September 2026, Hiroshima, Japan

From Ancient Legends to Pixels: Reconstructing Ancient Esna Landscape with GIS and Remote Sensing

Zhenhai Li[1], Jianqiao Liu[2]

[1] Department of History, Peking University, Beijing 100871, China; 2501110894@stu.pku.edu.cn
[2] Department of Geography, University at Buffalo, Buffalo, NY 14261, USA; jliu222@buffalo.edu

Keywords: Esna, ritual landscape, Copernicus DEM, Landsat, hydroscape, open-source GIS.

Abstract

This paper develops a text-driven reconstruction of the ritual landscape associated with the Festival of Seizing the Staff at Esna, Upper Egypt. Temple inscriptions are treated as relational evidence encoding sequence, adjacency, orientation, thresholds, and ritual function rather than as surveyed maps. Three historical hypotheses are tested: the Upper Place formed a nested elevated setting; Red Lake and Lake of Rebel's Fragment belonged to a connected northern hydroscape; and the inscriptions preserve relational rather than metric topography. The analysis integrates a 30 m Copernicus DEM GLO-30, five cloud-screened Sentinel-2 Level-2A dates, JRC Global Surface Water, and 32 Landsat Collection 2 Level-2 scenes grouped into six epochs from 1984–2025. A reproducible workflow derives slope, multi-scale topographic position, D8 drainage, Topographic Wetness Index, Height Above Nearest Drainage, MNDWI, hydrogeomorphic concordance, terrain profiles, landscape-class persistence, and Nile transect change. The corridor is predominantly low gradient: 69.5% of valid cells are at or below 2°, and 36.9% lie within 5 m of modelled drainage elevation under the primary network. Across the six Landsat epochs, mean landscape-class persistence is 0.943 and 90.0% of valid pixels have persistence of at least 0.8. At 13 measurable Nile transects, the endpoint-period median Jaccard overlap is 0.944 and median absolute centre shift is 15 m, with a local exception of 570 m. These results describe modern surface and river-planform persistence only; they do not demonstrate unchanged elevation, ancient geomorphic stability, or archaeological-site preservation.

1. Introduction

At Esna, Upper Egypt, ritual geography is preserved most clearly in texts rather than in an excavated network of monuments. The Temple of Khnum inscriptions describe named cult places, directions, approaches, lake edges, stopping points, and ordered processions. Their spatial information is therefore substantial, but it is theological and performative rather than equivalent to modern coordinates (Sauneron, 1962).

The Festival of Seizing the Staff, also known as the Victory Festival of Khnum, is especially suitable for a text-driven geospatial test. Figure 1 summarizes its mythic prologues, purification rules, three visits of Khnum to North Esna, and the Neith-related celebration. Figure 2 places the principal historical toponyms within the modern corridor and visualizes approximate inscription-derived distances. The points and lines are interpretive anchors, not surveyed archaeological boundaries; several North Esna cult places are lost or remain uncertain (Abdel-Rahman Ali, 2009; Hallof, 2011).

The study asks whether these relational statements are compatible with measured terrain and water settings, and whether their broader environmental framework persisted during the modern satellite record. Reconstruction is used in a constrained sense: it denotes a reproducible model of plausible spatial relations, not recovery of exact ancient coordinates. This distinction is essential because modern topography and surface water have been modified by irrigation, embankment, urban growth, channel engineering, and the Aswan High Dam.

Three questions guide the analysis: (1) what regional and local terrain contrasts characterize the Esna corridor; (2) where do drainage-relative elevation, wetness, low slope, and remotely observed water agree; and (3) how far do terrain relations and 1984–2025 landscape-surface persistence support H1–H3 without being converted into evidence of ancient elevation stability or archaeological-site preservation?

Figure 1. Event structure of the Festival of Seizing the Staff. The geospatial reconstruction begins from the ordered ritual sequence and named localities, not from isolated modern point identification.

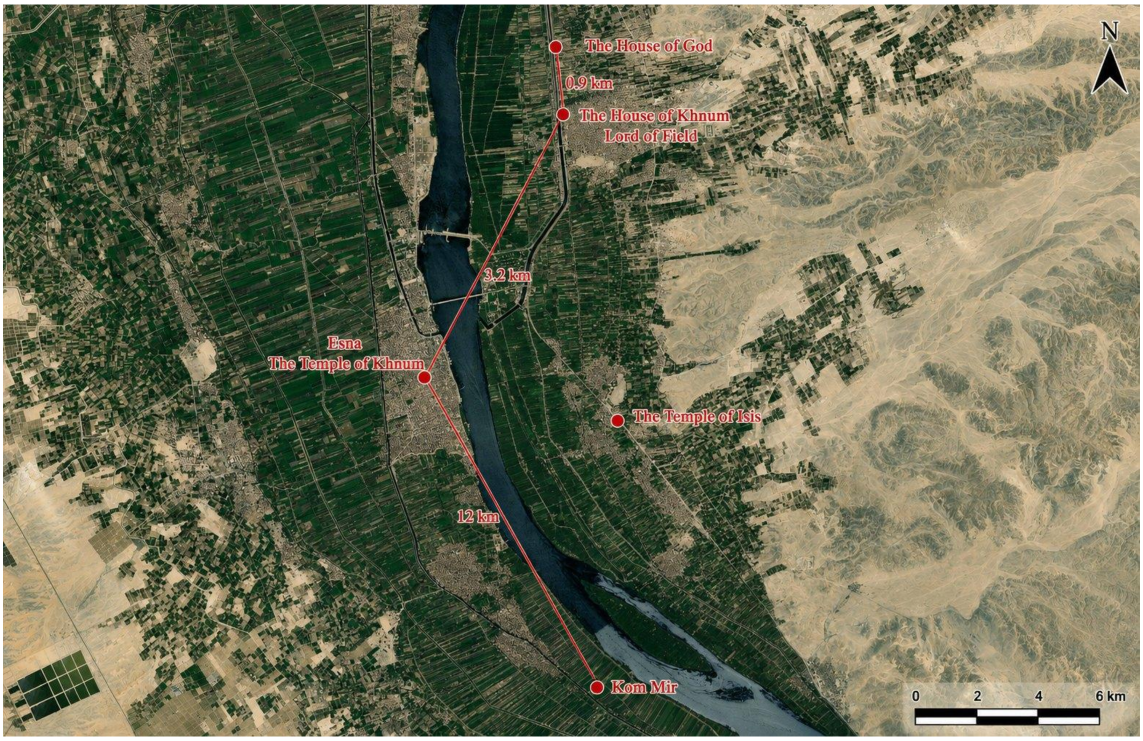

Figure 2. Author-compiled basemap of key Esna localities and inscription-derived distance relationships. Red labels denote the 0.9 km, 3.2 km, and 12 km relations reported or inferred from the inscriptions, not distances measured from the modern basemap. The central distance segment is schematic, so its drawn length differs visibly from the map-scale distance. Point placements are approximate and are not surveyed archaeological boundaries.

2. Historical Hypotheses and Text-Derived Spatial Logic

2.1 Festival Sequence as Spatial Evidence

The historical model begins with event order. In the first Khnum visit, the procession moves from Esna to the House of Khnum and then to the Upper Place, where sacrifice and praise are performed around a mound. In the second visit, movement proceeds through the House of God and the Upper Place before turning toward Red Lake and the edge of Lake of Rebel's Fragment. In the third visit, the sequence links the House of God, the path to the Shu Temple, and an orientation toward Lake of Rebel's Fragment. The Neith celebration introduces an Esna-centred riverfront subsystem between the temple and the Tribune on the Water (Sauneron, 1962).

These passages preserve sequence, adjacency, entrance, edge, facing, and return. They do not supply a complete metric network. The distance segments in Figure 2 are consequently treated as text-derived constraints rather than map-scale measurements; the central segment is schematic and its drawn length should not be compared directly with the modern basemap.

2.2 H1: Upper Place as a Nested Elevated Setting

H1 interprets the Upper Place as a broader elevated ritual zone containing a more localized mound-centred node. The text associates it with sacrifice, burial, divine dwelling, cavern-like imagery, and praise around a mound (Sauneron, 1962). The combination argues against reducing the toponym to one modern point, but it also does not justify equating it with the House of Khnum or the House of God. The defensible claim is a close topographic and ritual association among distinct places.

A 30 m surface model can test whether the floodplain contains relative highs, levee-like transitions, and elevated surfaces adjoining low drainage-relative ground. It cannot resolve a small mound, courtyard, buried structure, or ancient ground surface.

2.3 H2: Red Lake and Lake of Rebel's Fragment as a Linked Hydroscape

H2 treats Red Lake and Lake of Rebel's Fragment as differentiated but connected water sectors in a northern ritual field. The inscriptions distinguish entrance, edge, facing, protection, burial, and rebel-slaying (Sauneron, 1962). The spatial test is therefore not a search for one lost lake. It screens for low-gradient, low-HAND, high-TWI, and independently observed water-adjacent surfaces. Agreement raises hydrogeomorphic plausibility but does not establish age, name, ritual meaning, or archaeological identity.

2.4 H3 and the Operational Layer 1–3 Framework

H3 proposes that the inscriptions preserve relational rather than metric topography. Their evidential value lies in ordered movement, direction, adjacency, thresholds, symbolic elevation, and environmental contrast. GIS should test whether a proposed arrangement is geomorphologically possible, not claim that a text has been confirmed by a raster.

H1–H3 express the historical propositions, whereas Layers 1–3 define their geospatial operationalization. Layer 1 evaluates relative elevation and floodplain position through topographic position, slope, and HAND. Layer 2 evaluates water-edge plausibility through slope, HAND, TWI, Sentinel-2 MNDWI, JRC water history, and Landsat-era water frequency. Layer 3 evaluates the western and eastern margins through repeated east–west profiles. Table 1 summarizes the tests and their interpretive limits.

https://doi.org/10.5194/isprs-archives-L-4-W1-2026-383-2026 |

Historical proposition	Text-derived claim	Operational test	Interpretive limit
H1 / Layer 1	Upper Place as a broader elevated setting with a local node.	Slope; HAND; TPI at 300 m and 1,000 m.	Tests relative setting only; cannot identify a mound or temple.
H2 / Layer 2	Red Lake and Lake of Rebel's Fragment as linked water-oriented sectors.	Slope; HAND; TWI; Sentinel-2 MNDWI; JRC water; Landsat water frequency.	Screens modern hydrogeomorphic agreement; cannot date or name an ancient lake.
H3 / Layer 3	Sequence, adjacency, direction, and margins are more secure than exact metrics.	Five east–west profiles; river-planform transects; landscape persistence.	Tests regional relations and modern persistence; cannot establish an ancient route or elevation stability.

Table 1. Historical hypotheses translated into operational GIS and remote-sensing questions.

3. Data and Methods

3.1 Study Area, Grid, and Data Sources

The corridor covers 32.44–32.66° E and 25.14–25.48° N, including the Nile floodplain, Esna on the west bank, North Esna on the east bank, and adjacent desert margins. All common-grid products were transformed to WGS 84 / UTM zone 36N (EPSG:32636) and aligned to a 30 m grid of 1,258 × 743 cells. Historical point placements were not used as training or calibration locations because their archaeological positions are uncertain.

Terrain analysis used Copernicus DEM GLO-30, a digital surface model rather than a bare-earth archaeological terrain model (Copernicus, 2022). Sentinel-2 Level-2A observations comprised five cloud-screened dates from July–September 2023 and September–October 2024, mosaicked across MGRS tiles 36RVN and 36RVP (Drusch et al., 2012). JRC Global Surface Water v1.5 occurrence and maximum extent supplied Landsat-derived water observations for 1984–2024 (Pekel et al., 2016).

3.2 Terrain Conditioning and Hydrogeomorphic Variables

The DEM was conditioned by depression filling before D8 flow direction and flow accumulation were calculated (Jenson and Domingue, 1988; Eilander, 2020). Slope was reported in degrees. TWI represented the logarithmic relation between specific catchment area and local slope (Beven and Kirkby, 1979), while TPI was calculated at approximately 300 m and 1,000 m neighbourhoods to separate local and broader relative relief (Wilson and Gallant, 2000). HAND was calculated relative to drainage networks extracted at 1,000, 5,000, and 10,000 contributing cells; the 5,000-cell network was primary and the alternatives provided sensitivity bounds (Nobre et al., 2011).

A transparent 0–4 concordance score added one point for each of four conditions: slope ≤2°, HAND ≤5 m, TWI at or above the corridor 75th percentile, and JRC-detected water. The score is an unweighted screening index, not a probability of an ancient lake or site. Five east–west profiles at 25.18°, 25.25°, 25.32°, 25.39°, and 25.46° N compared western and eastern edge relief with a central zone.

3.3 Sentinel-2 and JRC Water Observations

Sentinel-2 bottom-of-atmosphere reflectance was masked with the scene-classification layer, excluding no-data, defective, shadow, cloud, cirrus, and snow/ice classes. A median composite was generated after harmonizing the source bands to the common grid. MNDWI was calculated from green and SWIR1 reflectance following Xu (2006). Its role was to characterize modern water contrast, while JRC occurrence and maximum extent supplied an independent multi-decadal observation envelope. Neither product was treated as palaeohydrological dating.

3.4 Landsat 1984–2025 Surface-Persistence Analysis

USGS Landsat Collection 2 Level-2 surface reflectance was organized into six sensor-era epochs: 1984–1988, 1992–1996, 1999–2002, 2008–2011, 2014–2018, and 2021–2025. The analysis used 32 Tier-1 scenes: five scenes in epochs 1–3 and 6, and six in epochs 4–5. Landsat 4–5 TM, Landsat 7 ETM+, and Landsat 8–9 OLI products were cited and processed as their respective Collection 2 datasets (Earth Resources Observation and Science Center, 2020a, 2020b, 2020c).

The USGS product identifiers were accessed through the public Microsoft Planetary Computer STAC mirror (Microsoft Open Source et al., 2022). Only AOI windows were read from cloud-optimized GeoTIFFs. Surface-reflectance integers were converted using the metadata scale 0.0000275 and offset −0.2. QA_PIXEL bits 0–5 removed fill, dilated cloud, cirrus or the sensor-specific unused bit, cloud, shadow, and snow; QA_RADSAT had to equal zero, and reflectance outside 0–1 was rejected.

Epoch	Date span	Sensor(s)	Scenes	Valid (%)	MNDWI threshold	Water (%)	Median NDVI
E1	1984-07-11–1988-08-07	L5 TM	5	92.7	0.004	2.70	0.092
E2	1992-07-17–1996-08-13	L5 TM	5	100.0	0.010	2.25	0.093
E3	1999-07-05–2002-07-05	L5 TM; L7 ETM+	5	100.0	−0.045	2.50	0.078
E4	2008-07-13–2011-07-06	L5 TM	6	89.3	−0.032	2.77	0.077
E5	2014-07-30–2018-09-11	L8 OLI	6	100.0	−0.115	2.18	0.109
E6	2021-07-17–2025-09-06	L8–9 OLI	5	100.0	−0.066	2.12	0.116

Table 2. Landsat epoch composites. Valid percentage is the fraction of the AOI represented in each composite; thresholds are epoch-specific Otsu MNDWI values.

Within each epoch, median green, red, NIR, and SWIR1 reflectance, interquartile range, and valid-observation count were produced, followed by NDVI, MNDWI, and NDBI. Because TM/ETM+ and OLI have different spectral responses, raw cross-sensor reflectance was not interpreted as direct change (Roy et al., 2016). Water used an epoch-specific Otsu threshold (Otsu, 1979) estimated inside a 500 m JRC maximum-water buffer, clipped to [−0.15, 0.15], combined with NDVI <0.30, and filtered to components of at least three pixels. Fixed MNDWI thresholds of −0.05, 0, and 0.05 tested sensitivity.

Landscape classes were water, vegetation (NDVI ≥0.20), and other. Pixel persistence was the fraction of valid epochs occupied by the modal class and required at least five epochs. Main-Nile width and centre were measured at 16 fixed latitudes between 25.16° and 25.46° N. Early–late overlap used the Jaccard index.

This contribution has been peer-reviewed.
https://doi.org/10.5194/isprs-archives-L-4-W1-2026-383-2026

Associations between six-epoch water frequency and HAND, TWI, or slope were estimated with Spearman correlation on 1 km block means; 95% intervals used 1,000 block-bootstrap replicates with seed 20260724. Masked normalized cross-correlation of margin NDVI checked integer-pixel registration against 2021–2025.

3.5 Evaluation Logic

The historical hypotheses were evaluated by convergence rather than calibration. No terrain threshold was adjusted to reproduce an uncertain ancient locality. H1 was assessed through relative highs adjoining drainage-relative low ground; H2 through agreement among terrain wetness, observed water, and modern Landsat water frequency; and H3 through profiles, broad river-planform relations, and the distinction between persistent environmental structure and exact coordinates. Results were classified as support for setting, ambiguity, or contradiction, never as site identification.

4. Results

4.1 Regional Terrain and Drainage-Relative Elevation

Valid DEM elevation ranges from 71.0 to 668.3 m. The corridor is predominantly low gradient: 69.49% of valid cells have slope 0–2°, 13.64% have 2–5°, 6.50% have 5–10°, 6.85% have 10–20°, and 3.52% exceed 20°. Figure 3 shows the strong separation between the low Nile corridor and dissected desert margins, together with large internal variation in drainage-relative elevation and concordance.

HAND is sensitive to drainage definition, as expected. Under the primary 5,000-cell network, median HAND is 9.50 m and 36.9% of valid cells lie within 5 m of modelled drainage elevation. The 1,000-cell network increases this share to 51.0%, while the 10,000-cell network reduces it to 31.7% (Table 3). Concordance scores 3–4 occupy 16.32% of valid cells. These are the strongest modern terrain-water agreement zones, not classified ancient lakes or sites.

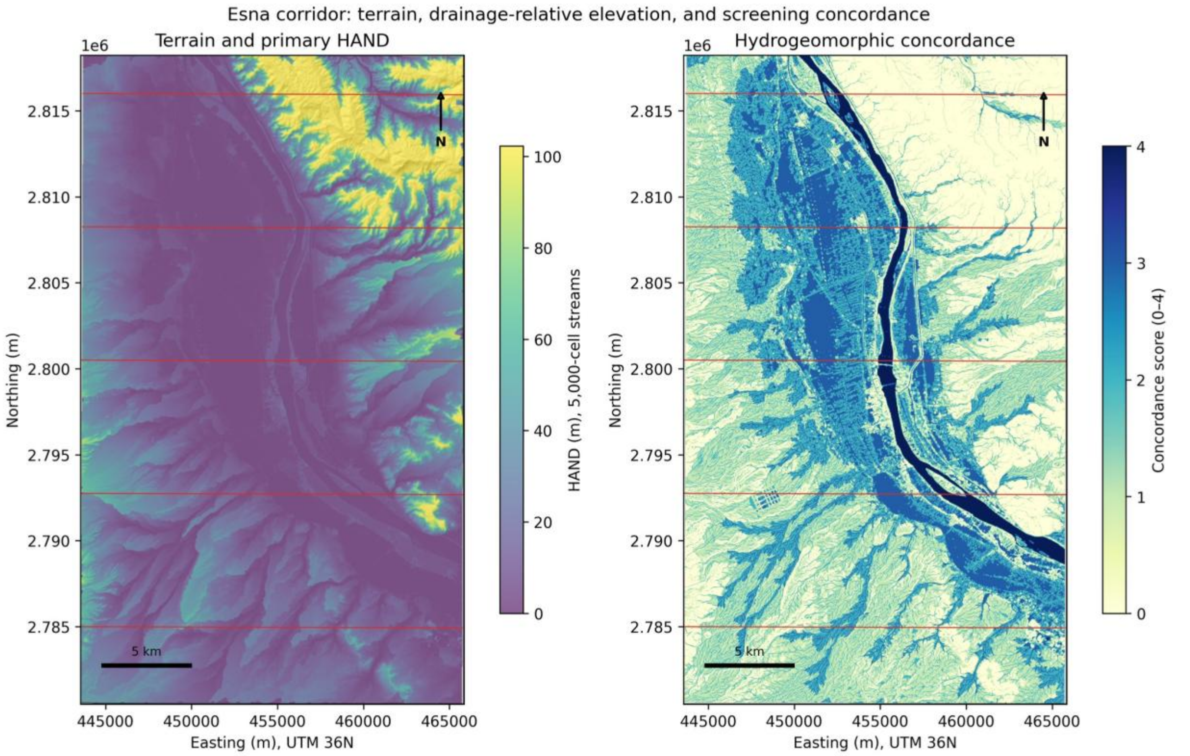

Figure 3. Copernicus DEM-derived terrain, primary HAND (5,000-cell drainage threshold), and unweighted 0–4 hydrogeomorphic concordance. Red profile lines mark the five east–west tests. The score is a screening index, not an archaeological probability.

Stream threshold	Median HAND (m)	≤2 m (%)	≤5 m (%)	≤10 m (%)
1,000 cells	4.80	34.8	51.0	69.0
5,000 cells (primary)	9.50	26.1	36.9	51.2
10,000 cells	12.93	22.7	31.7	44.8

Table 3. HAND sensitivity to drainage-network definition.

4.2 Sentinel-2 and JRC Water Agreement

JRC water occurrence above zero covers 2.91% of the corridor and maximum water extent covers 2.96%. The Sentinel-2 median composite contains 0.94% positive-MNDWI pixels; 99.7% of those pixels fall within the JRC-detected water mask. Figure 4 therefore shows strong agreement for persistent open water, chiefly the Nile, while low or negative MNDWI elsewhere does not exclude seasonal, historical, irrigated, or buried water-related settings.

https://doi.org/10.5194/isprs-archives-L-4-W1-2026-383-2026

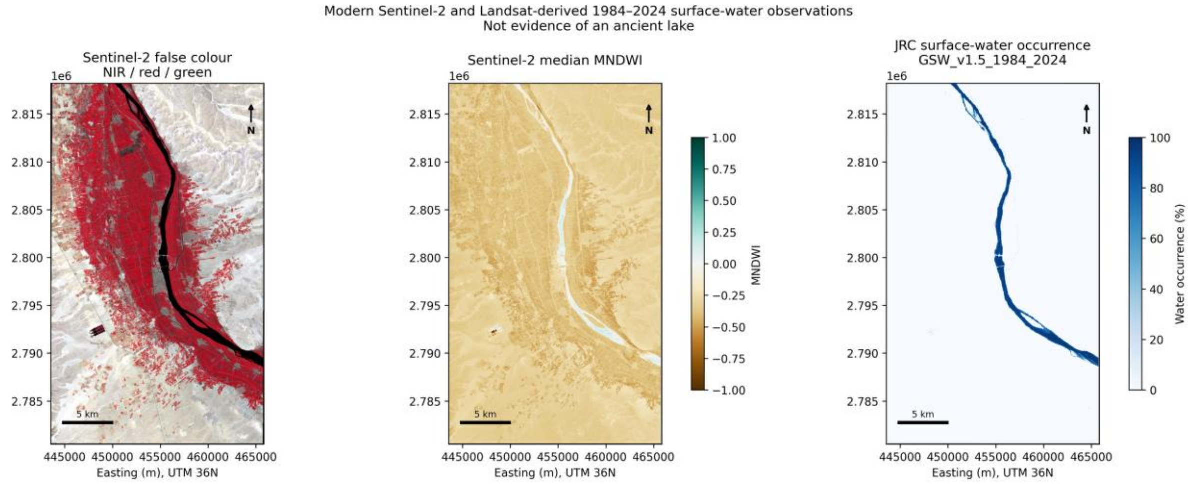

Figure 4. Modern multispectral and long-term surface-water observations: Sentinel-2 false-colour composite, median MNDWI, and JRC Global Surface Water occurrence for 1984–2024. These layers constrain the surviving modern hydroscape and do not locate an ancient lake.

4.3 Landsat-Era Surface Persistence and Nile Planform

All six epochs satisfied the four-scene minimum, with 32 selected scenes and 89.3–100.0% valid composite coverage (Table 2). The mean modal landscape-class persistence across 874,750 pixels observed in at least five epochs is 0.943; 90.0% of those pixels retain their modal class in at least 80% of valid epochs. Persistence is spatially structured. The lowland mean is 0.919 and 85.8% of lowland pixels reach 0.8 persistence, whereas the margin mean is 0.995 and 98.9% reach 0.8. Early–late class change affects 23.1% of the lowland but only 1.5% of the margin. The result is a persistent modern valley-margin framework with greater surface dynamism in cultivated and channel-adjacent lowlands.

Across comparable endpoint pixels, 2.2% are stable water, 0.5% water loss, and 0.1% water gain. Fixed MNDWI alternatives changed epoch water fractions by no more than 0.11 percentage points from the primary masks. The registration check found a maximum integer displacement of 0 pixels relative to 2021–2025, so no correction was applied.

Thirteen of the 16 requested main-Nile transects are measurable in both endpoint epochs. Their median early–late Jaccard overlap is 0.944, median absolute centre shift is 15 m, and median width change is −30 m. These medians indicate broad planform persistence at the measurable transects, but not spatial uniformity: the maximum local centre shift is 570 m at 25.22° N, and several other transects show substantially lower overlap. The three southern transects at 25.16°, 25.18°, and 25.20° N contain no valid river run in one or both endpoint epochs and are not assigned zero change.

At the 1 km block-mean grain, six-epoch water frequency is negatively associated with HAND (ρ=−0.222, 95% bootstrap CI [−0.266, −0.176]) and positively associated with TWI (ρ=0.304 [0.248, 0.356]). The slope association is near zero (ρ=0.015 [−0.036, 0.064]). Thus drainage-relative elevation and accumulated wetness explain modern water recurrence more clearly than slope alone. Table 4 reports the exact Landsat-era diagnostics and their evidential scope; Figure 5 summarizes the epoch, persistence, transect, and terrain-association results.

Diagnostic	Estimate	Interpretive scope
Epochs / selected scenes	6 / 32	All planned epochs passed the four-scene minimum.
Mean class persistence	0.943	Modern three-class surface framework only.
Pixels with persistence ≥0.8	90.0%	Valid pixels observed in at least five epochs.
Lowland / margin persistence	0.919 / 0.995	Lowlands are more dynamic than desert margins.
Stable / lost / gained water	2.2 / 0.5 / 0.1%	Comparable early–late AOI pixels.
Measurable transects	13 / 16	Three southern transects were unmeasurable.
Median Jaccard / absolute shift	0.944 / 15 m	Broad median planform persistence.
Maximum shift / median width change	570 m / −30 m	Local exception rules out uniform stability.
HAND ρ (95% CI)	−0.222 [−0.266, −0.176]	Spearman association on 1 km block means.
TWI ρ (95% CI)	0.304 [0.248, 0.356]	Positive association with modern water frequency.
Slope ρ (95% CI)	0.015 [−0.036, 0.064]	No clear independent block-scale association.

Table 4. Landsat-era persistence, Nile-planform, and terrain-association diagnostics. Claims concern modern observations only.

Epoch-specific water fractions remain within 2.12–2.77% of valid composite pixels, although the primary MNDWI threshold varies from 0.010 to −0.115 across sensor eras. Repeating the classification at fixed thresholds of −0.05, 0, and 0.05 changes an epoch water fraction by at most 0.11 percentage points. This stability in mapped area supports use of the primary masks for broad comparison, while the threshold variation cautions against treating one raw MNDWI value as sensor-invariant. Median NDVI ranges from 0.077 to 0.116 and classified vegetation from 26.7% to 39.6%; these values describe the six composites and are not interpreted as a continuous ecological trend.

The transect distribution also qualifies the medians. Eight of 13 measurable transects have Jaccard overlap of at least 0.90, and 10 have absolute centre displacement no greater than one 30 m pixel. The remaining three measured shifts are 165, 195, and 570 m, and the lowest overlap is 0.116. Thus the main-Nile result is a strong central tendency with explicit local exceptions, not a claim that every reach remained fixed.

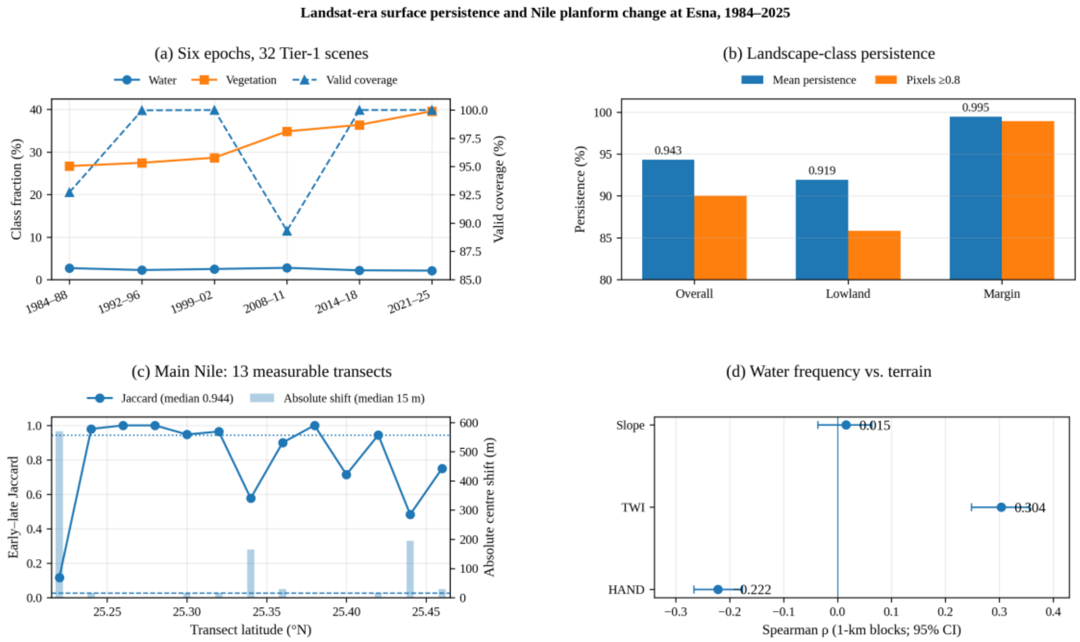

Figure 5. Landsat-era surface persistence and Nile planform change at Esna, 1984–2025. Panels summarize six epoch composites (32 scenes), modal landscape-class persistence, endpoint-period river overlap and centre shift at 13 measurable transects, and 1 km block-mean terrain correlations with 95% bootstrap intervals. Results concern modern remotely sensed surface patterns and river planform, not unchanged elevation or ancient stability.

4.4 Layer 3 Profile Test

The five profiles in Figure 6 do not support a consistent 200–300 m western ridge. Western edge 95th-percentile relief relative to the central comparison zone ranges from −47.5 to 86.4 m. Eastern edge relief ranges from −26.1 to 473.1 m and increases sharply in the northern profiles. Around central Esna, both margins rise by tens rather than hundreds of metres; farther north, eastern desert relief becomes much larger. Layer 3 is therefore a heterogeneous regional boundary, not a single Western Mountains landform with a stable magnitude.

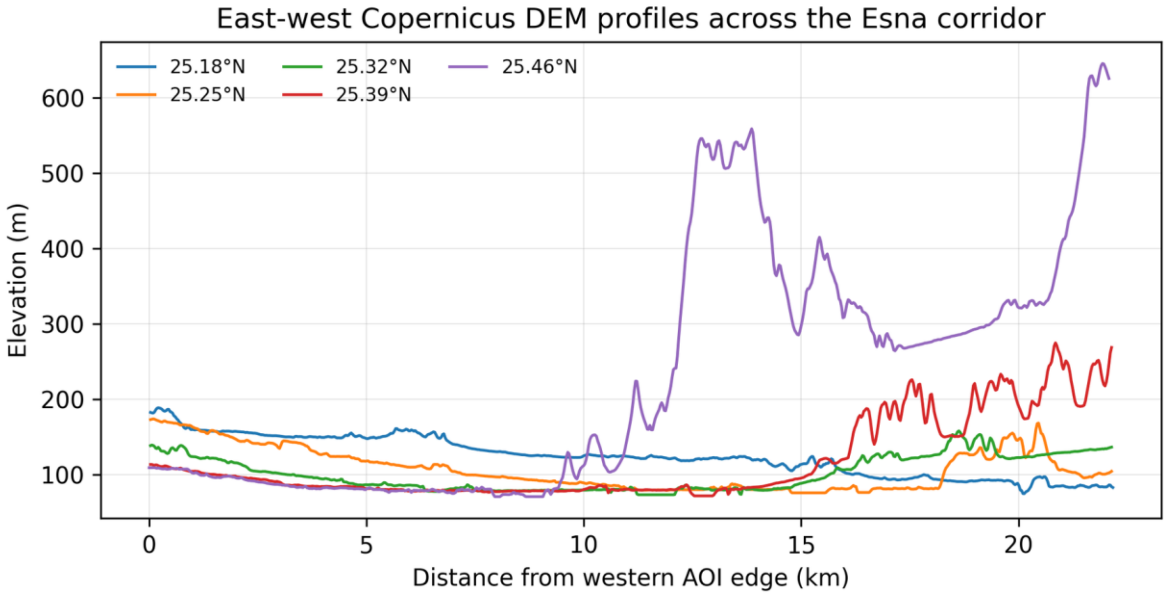

Figure 6. Five east–west Copernicus DEM profiles across the Esna corridor. Relief is strongly heterogeneous and does not define a consistent 200–300 m western ridge.

4.5 Evaluation of H1–H3

H1 is supported only at the level of setting. Multi-scale TPI and HAND show relative highs beside drainage-relative low ground within a broadly low corridor, compatible with a nested elevated ritual zone. The data cannot identify the Upper Place or its mound. H2 receives broader environmental support: low slope, low HAND, high TWI, modern Sentinel-2/JRC water, and

Landsat water frequency converge along the Nile and selected lowland surfaces. This is compatible with a connected water-oriented field but cannot name or date Red Lake or Lake of Rebel’s Fragment.

H3 is most strongly supported as a method of interpretation. The inscriptions can be translated into sequences, margins, and environmental relations without forcing exact coordinates. Modern landscape classes and median river planform are persistent enough to retain a recognizable valley–river–margin framework across 1984–2025, while local river exceptions and lowland class change show why metric literalism remains unsafe.

5. Discussion

5.1 Integrating Historical and Geospatial Evidence

The combined workflow clarifies the division of evidence. Historical sources name places, functions, and ordered relations; the DEM measures present surface form and drainage-relative position; Sentinel-2, JRC, and Landsat constrain modern water and surface patterns. No uncertain historical point was used to train or calibrate a terrain threshold. Agreement therefore means that a text-derived environmental relation is compatible with measured modern conditions, while ambiguity remains visible.

This separation makes the Layer 1–3 framework useful without turning it into a deterministic site model. Layer 1 identifies combinations of relative height and lowland adjacency that could accommodate the broad language of an Upper Place. Layer 2 identifies persistent or recurrent water-related settings. Layer 3 tests regional contrasts and demonstrates their spatial heterogeneity. The result narrows defensible setting types rather than selecting archaeological pixels.

5.2 What the Landsat Record Does—and Does Not—Show

The Landsat analysis provides a temporal test of modern landscape-surface persistence. The modal three-class framework is highly persistent overall and especially along the desert margins, whereas lowlands are more dynamic. The median main-Nile overlap and 15 m centre shift support broad endpoint-period planform persistence at measurable transects, but the 570 m exception and three unmeasurable southern transects preclude a uniform-stability claim.

Optical reflectance does not measure elevation change. Consequently, the analysis cannot demonstrate that topographic height remained unchanged, exclude erosion or channel migration outside the sampled periods, establish millennial or ancient geomorphic stability, or infer preservation of archaeological remains. The 1984–2025 record instead shows that a recognizable modern valley–river–margin surface framework persisted while channel-adjacent and cultivated lowlands changed more frequently.

5.3 Reassessment of the Marginal Mountains

The profiles do not support a uniform 200–300 m characterization of the Western Mountains. Western relief is generally modest relative to the central corridor, whereas the eastern margin becomes much higher toward the north. Inscriptional language of an absolute or protective boundary may still have phenomenological or symbolic force, but the present profiles do not support one average ridge height or one metrically literal landform.

5.4 Limitations and Uncertainty

All geospatial evidence is temporally displaced from the temple texts. Copernicus DEM is a modern digital surface model; Sentinel-2 represents 2023–2024; JRC summarizes detections from 1984–2024; and Landsat is represented by six multi-year snapshots rather than annual mapping. Irrigation, urbanization, embankment, channel engineering, and dam regulation affect the observed surface. Thirty-metre mixed pixels cannot resolve small mounds, narrow canals, temple platforms, courtyards, or buried architecture.

Hydrological conditioning on a clipped corridor truncates some upstream area, and HAND depends on network threshold. Landsat uncertainty includes seasonal compositing, residual atmospheric effects, cross-sensor response differences, Otsu threshold choice, and JRC-guided river selection. The block bootstrap addresses spatially dense pixel counts but does not remove these observational limits. Finally, approximate historical anchors prevent defensible least-cost routing or exact processional reconstruction.

6. Conclusions

This study reconstructs the Festival of Seizing the Staff as a text-driven GIS and remote-sensing problem. The historical evidence is preserved as sequence, adjacency, direction, entrance, edge, and ritual function. The geospatial evidence is limited to present terrain form, drainage-relative elevation, wetness tendency, and modern surface-water and landscape observations.

Three conclusions follow. First, the Upper Place is most defensibly treated as a nested elevated setting within a broader lowland landscape, although the 30 m surface model cannot identify a mound or cult place. Second, multiple terrain-water indicators support the broad plausibility of a connected northern hydroscape, but they cannot locate or date the named lakes. Third, H3 provides the strongest bridge between text and measurement: the modern valley–river–margin framework shows high 1984–2025 surface persistence and median Nile planform persistence, yet local exceptions and changing lowlands rule out claims of uniform or ancient stability. The five-profile test also rejects a uniform 200–300 m western ridge.

The resulting reconstruction is therefore a constrained model of environmental plausibility. It demonstrates how open data, transparent access records, and reproducible processing can strengthen historical reasoning without replacing it or converting modern observations into archaeological proof.

Acknowledgements and Data Availability

Produced using Copernicus WorldDEM-30 © DLR e.V. 2010–2014 and © Airbus Defence and Space GmbH 2014–2018, provided under COPERNICUS by the European Union and ESA. Sentinel-2 figures contain modified Copernicus Sentinel data. JRC attribution: Source EC JRC/Google. Landsat Collection 2 Level-2 imagery is courtesy of the U.S. Geological Survey and was accessed through the Microsoft Planetary Computer public STAC mirror. Analysis code, product identifiers, and supporting tables are archived in the project repository.

References

Abdel-Rahman Ali, M., 2009. The Lost Temples of Esna. *Bulletin de l'Institut français d'archéologie orientale*, 109, 1–8.

Beven, K.J., Kirkby, M.J., 1979. A physically based, variable contributing area model of basin hydrology. *Hydrological Sciences Bulletin*, 24(1), 43–69. doi.org/10.1080/02626667909491834.

Copernicus, 2022. Copernicus Digital Elevation Model (DEM), GLO-30. European Space Agency. doi.org/10.5270/ESA-c5d3d65.

Drusch, M., Del Bello, U., Carlier, S., Colin, O., Fernandez, V., Gascon, F., Hoersch, B., Isola, C., Laberinti, P., Martimort, P., Meygret, A., Spoto, F., Sy, O., Marchese, F., Bargellini, P., 2012. Sentinel-2: ESA's optical high-resolution mission for GMES operational services. *Remote Sensing of Environment*, 120, 25–36.
doi.org/10.1016/j.rse.2011.11.026.

Earth Resources Observation and Science (EROS) Center, 2020a. Landsat 4–5 Thematic Mapper Level-2, Collection 2 [dataset]. U.S. Geological Survey.
doi.org/10.5066/P9IAXOVV.

Earth Resources Observation and Science (EROS) Center, 2020b. Landsat 7 Enhanced Thematic Mapper Plus Level-2, Collection 2 [dataset]. U.S. Geological Survey.
doi.org/10.5066/P9C7I13B.

Earth Resources Observation and Science (EROS) Center, 2020c. Landsat 8–9 Operational Land Imager/Thermal Infrared Sensor Level-2, Collection 2 [dataset]. U.S. Geological Survey.
doi.org/10.5066/P9OGBGM6.

Eilander, D., 2020. pyflwdir: Fast methods to work with hydro- and topography data in pure Python. Zenodo.
doi.org/10.5281/zenodo.4287338.

Hallof, J., 2011. The Temple of Esna North. In: Wendrich, W. (Ed.), *UCLA Encyclopedia of Egyptology*. University of California, Los Angeles.
escholarship.org/uc/item/2018g2c8 (30 July 2026).

Jenson, S.K., Domingue, J.O., 1988. Extracting topographic structure from digital elevation data for geographic information system analysis. *Photogrammetric Engineering & Remote Sensing*, 54(11), 1593–1600.

Microsoft Open Source, McFarland, M., Emanuele, R., Morris, D., Augspurger, T., 2022. microsoft/PlanetaryComputer: October 2022, version 2022.10.28. Zenodo.
doi.org/10.5281/zenodo.7261897.

Nobre, A.D., Cuartas, L.A., Hodnett, M., Rennó, C.D., Rodrigues, G., Silveira, A., Waterloo, M.J., Saleska, S., 2011. Height Above the Nearest Drainage—A hydrologically relevant new terrain model. *Journal of Hydrology*, 404(1–2), 13–29.
doi.org/10.1016/j.jhydrol.2011.03.051.

Otsu, N., 1979. A threshold selection method from gray-level histograms. *IEEE Transactions on Systems, Man, and Cybernetics*, 9(1), 62–66.
doi.org/10.1109/TSMC.1979.4310076.

Pekel, J.-F., Cottam, A., Gorelick, N., Belward, A.S., 2016. High-resolution mapping of global surface water and its long-term changes. *Nature*, 540, 418–422.
doi.org/10.1038/nature20584.

Roy, D.P., Kovalskyy, V., Zhang, H.K., Vermote, E.F., Yan, L., Kumar, S.S., Egorov, A., 2016. Characterization of Landsat-7 to Landsat-8 reflective wavelength and normalized difference vegetation index continuity. *Remote Sensing of Environment*, 185, 57–70.
doi.org/10.1016/j.rse.2015.12.024.

Sauneron, S., 1962. *Les fêtes religieuses d'Esna aux derniers siècles du paganisme (Esna V)*. Institut français d'archéologie orientale, Cairo.

Wilson, J.P., Gallant, J.C., 2000. *Terrain Analysis: Principles and Applications*. John Wiley & Sons, New York.

Xu, H., 2006. Modification of normalised difference water index (NDWI) to enhance open water features in remotely sensed imagery. *International Journal of Remote Sensing*, 27(14), 3025–3033.
doi.org/10.1080/01431160600589179.

Appendix A. Main-Nile Endpoint Transect Diagnostics

Latitude (°N)	Jaccard	Centre shift (m)	Width change (m)	Status
25.16	—	—	—	Unmeasurable
25.18	—	—	—	Unmeasurable
25.20	—	—	—	Unmeasurable
25.22	0.116	−570	−840	Measured
25.24	0.979	−15	−30	Measured
25.26	1.000	0	0	Measured
25.28	1.000	0	0	Measured
25.30	0.947	15	−30	Measured
25.32	0.964	15	−30	Measured
25.34	0.577	165	−330	Measured
25.36	0.900	30	0	Measured
25.38	1.000	0	0	Measured
25.40	0.714	0	−120	Measured
25.42	0.944	15	−30	Measured
25.44	0.483	195	−450	Measured
25.46	0.750	30	−120	Measured

Table A1. Early (1984–1988) versus late (2021–2025) main-Nile transect diagnostics. Centre shifts retain the signed analysis convention; the main text reports their absolute median. Blank metrics indicate no valid river run in one or both endpoint epochs.